

Supplementary information for “Nonreciprocal directional dichroism of a chiral magnet in the visible range”

M. O. Yokosuk,¹ Heung-Sik Kim,^{2,3} K. D. Hughey,¹ Jaewook Kim,^{2,4} A. V. Stier,⁵ K. R. O’Neal,¹ Junjie Yang,⁶ S. A. Crooker,⁵ K. Haule,² Sang-Wook Cheong,^{2,4,7} David Vanderbilt,² and J. L. Musfeldt^{1,8,*}

¹*Department of Chemistry, University of Tennessee, Knoxville, Tennessee 37996, USA*

²*Department of Physics and Astronomy, Rutgers University, Piscataway, New Jersey 08854, USA*

³*Department of Physics, Kangwon National University, Chuncheon 24341, Korea*

⁴*Rutgers Center for Emergent Materials, Rutgers University, Piscataway, New Jersey 08854, USA*

⁵*National High Magnetic Field Laboratory, Los Alamos, New Mexico 87545, USA*

⁶*Department of Physics and The Science of Advanced Materials Program,
Central Michigan University, Mount Pleasant, Michigan 48858, USA*

⁷*Laboratory for Pohang Emergent Materials and Max Planck POSTECH Center for Complex Phase Materials,
Pohang University of Science and Technology, Pohang 790-784, Korea*

⁸*Department of Physics and Astronomy, University of Tennessee, Knoxville, Tennessee 37996, USA*

Summary of symmetry arguments

We first consider configurations in which a chiral axis C , external magnetic field H , and propagation direction k are mutually parallel or orthogonal, with polarization P absent. From a symmetry standpoint, only two such configurations, the ones measured in the present work, can show a nonreciprocal effect. Specifically, nonreciprocal direction dichroism (NDD) can emerge only when $H \parallel k$, while H and k are both either parallel (magneto-chiral orientation) or orthogonal (transverse magneto-chiral orientation) to C . When all three (C , H , and k) are orthogonal, no nonreciprocal effect will emerge, as a C_2 rotation about the H axis reverses k but not C or H . Table S1 lists all possible relative orientations of C , H , and k , ignoring global rotations (i.e., the configuration $\uparrow C, \uparrow H, \leftrightarrow k$ could be rewritten as $\leftrightarrow C, \leftrightarrow H, \uparrow k$; in either case a C_2 rotational symmetry element reverses k while leaving the other orders invariant).

The story becomes different when polarization P is nonzero, but chirality C is absent. When P , H , and k are all orthogonal, a nonreciprocal effect can emerge – deemed toroidal dichroism. All other configurations, as shown in Table S2, have at least one symmetry that prevents the emergence of NDD. Again, we list only configurations that are unique under global rotation. Note that while only one relevant symmetry is listed in the table, others may perform the same function. For the case of $\uparrow P, \uparrow H, \leftrightarrow k$, for example, either a C_2 rotation about H or a mirror reflection across the k - H plane composed with time reversal will reverse k without reversing the other orders.

Finally, when both C and P exist simultaneously, the symmetry is lowered, so any situation (from either Table S1 or S2) that shows a nonreciprocal response is still valid for simultaneous C and P . Note that all

TABLE S1: Summary of all configurations including C , H , and k in the absense of P , indicating whether or not a nonreciprocal effect can emerge. If not, the symmetry that prevents it is given; if so, the name of the type of dichroism is given.

Configuration	NDD	Symmetry	Dichroism type
$\otimes C, \uparrow H, \leftrightarrow k$	No	C_2 about H	–
$\uparrow C, \uparrow H, \leftrightarrow k$	No	C_2 about H	–
$\leftrightarrow C, \uparrow H, \leftrightarrow k$	No	C_2 about H	–
$\leftrightarrow C, \leftrightarrow H, \leftrightarrow k$	Yes	–	Magneto-chiral
$\uparrow C, \leftrightarrow H, \leftrightarrow k$	Yes	–	Transverse magneto-chiral

TABLE S2: Summary of all configurations including P , H , and k in the absense of C , indicating whether or not a nonreciprocal effect can emerge. If not, the symmetry that prevents it is given; if so, the name of the type of dichroism is given. M indicates mirror; $M \otimes \text{TR}$ indicates mirror composed with time reversal.

Configuration	NDD	Symmetry	Dichroism type
$\otimes P, \uparrow H, \leftrightarrow k$	Yes	–	Toroidal
$\uparrow P, \uparrow H, \leftrightarrow k$	No	C_2 about H	–
$\leftrightarrow P, \uparrow H, \leftrightarrow k$	No	(M across k - H plane) \otimes TR	–
$\leftrightarrow P, \leftrightarrow H, \leftrightarrow k$	No	(M across plane containing k) \otimes TR	–
$\uparrow P, \leftrightarrow H, \leftrightarrow k$	No	M across plane $\perp k$	–

three NDD cases discussed above do have symmetry operational similarity (SOS) with k , the same broken symmetries of k , in the language of Ref. [S1].

The arguments above are generalized. Of course, Ni_3TeO_6 has both a static electric polarization P as well as a chiral axis C . A C_2 rotation is not, however, a relevant symmetry of the crystal structure because of the polarization. For materials like Ni_3TeO_6 with both P and C , all three of the aforementioned cases still apply. This includes nonreciprocal effects in the magneto-chiral, transverse magneto-chiral, and toroidal orientations. Ni_3TeO_6 therefore presents an opportunity to compare the two different versions of the magneto-chiral response in the same material.

Evidence for a single chiral domain in our polished crystals

Since Ni_3TeO_6 can show chiral domains throughout a polished sample [S2], it is important to confirm that our sample contains a single chiral domain. The different chiral domains can be revealed using a transmission optical microscope with a polarizer and analyzer. When the polarizer and analyzer are at slightly different angles, the light throughput reveals lighter and darker green regions indicating different chiral domains. Figure 1(d) in the main text shows the microscope image of the crossed polarizer measurement of

the *ab*-plane crystal, where we see two different chiral domains, indicated by the large light green portion and the dark green triangles at two different corners of the crystal. For our measurements, we expose the center of the crystal, indicated by the red circle in the figure. Hence, we can confirm that we measured a single chiral domain. Figure 1(e) shows an optical rotation measurement using crossed polarizer and analyzer (schematic within the panel). The angle Θ corresponds to the angle between the analyzer and normal from the polarizer. With the red data points corresponding to the lighter green portion of the crystal, we determine that a majority of the crystal contains right-handed chirality, as it has a positive value of Θ . Therefore, the small darker green triangles to have left-handed chirality with a negative Θ (as shown by the blue data points). Figure 1(g) is a photographic image under crossed polarizers of a polished single crystal that exposes the *c*-axis. If the sample was not polished to reveal a perfect *c*-axis in-plane, then color differentiation would emerge when using the polarizer/analyzer test. However, we see very little to no color difference. Again, the red circle indicates the portion of the crystal that was exposed to light during our measurements.

Since Ni_3TeO_6 has such low symmetry, a number of different optical effects can arise that could be confused with nonreciprocity. We tested for several of them. One example of such an optical phenomena that we tested for is natural optical rotation. In the *ab*-plane crystal, natural optical rotation certainly arises [Fig. 1(d)]. This has been explained in more detail above. However, for the crystal containing the *c*-axis (the crystallographic chiral axis) in the polished plane, there is no natural optical rotation observed within our sensitivity. Furthermore, natural optical activity as well as magnetic dichroism can be excluded from possible interpretations of the data since we use unpolarized light, and neither effect can account for nonreciprocal absorption of unpolarized light. In particular, (i) forward R-circular and reverse L-circular light waves display the same magnetic dichroism (and vice versa), so magnetic dichroic activity should not be responsible for our measurement. (ii) Natural optical rotation also does not depend on the light propagating direction. Since we used unpolarized light, our measured $\alpha(+H, \pm k)$ is an integration of polarization-dependent absorption $\alpha(\sigma, +H, \pm k)$ over all polarization σ . So the natural optical effect in $\alpha(+H, +k) - \alpha(+H, -k) = \int d\sigma [\alpha(\sigma, +H, +k) - \alpha(\sigma, +H, -k)]$ again cancels out σ -wise.

Spin-orbit coupling effects in optical absorption

A common misconception in 3*d* transition metal oxides is that the effect of atomic spin-orbit coupling on the electronic and magnetic properties is marginal, especially for Ni_3TeO_6 in its orbitally inert Ni^{2+} high-spin ($S = 1$) d^8 configuration. In the excitation channels, however, spin-orbit coupling may induce significant changes in optical transitions involving $t_{2g}^5 e_g^3$ excited configurations with an open t_{2g} shell. This is evident from the fact the nonreciprocal absorption discussed in the manuscript necessarily requires spin-orbit coupling. Not surprisingly, spin-orbit coupling also affects the absorption spectrum itself.

Figure S1(a, b) displays the theoretically-predicted absorption spectrum of Ni_3TeO_6 both with and without spin-orbit coupling. We projected the contribution of the three different Ni centers explicitly. All of these features are Ni on-site d -to- d excitations [S3], the specific assignments of which are given above panel (a). The excitations from 0.8 to 1.3 eV and from 1.5 to 2.0 eV, identified as ${}^3A_{2g} \rightarrow {}^3T_{2g}$ and ${}^3A_{2g} \rightarrow {}^3T_{1g}$ respectively, originate from one- and two-electron excitation from Ni t_{2g} to e_g orbitals respectively. Hence the excitation energies roughly correspond to the magnitude of the t_{2g} - e_g splitting and its doubling. In our calculation, similar to the previous theoretical estimates [S3], the computed multiplet excitations are slightly blue-shifted. This means that the cubic crystal field strength is slightly overestimated in our results, which does not affect overall messages though.

Figure S1(f) displays the magneto-optical response of Ni_3TeO_6 in the AFM, SF, and MM phases. These curves are presented as absorption differences, $\Delta\alpha = \alpha(E, H) - \alpha(E, H = 0)$, in order to highlight subtle field-induced spectral changes. The clearest indication of the phase and the largest changes are near 1.4 eV. Theoretical simulations - with and without spin-orbit coupling - are presented in Fig. S1(d,e) [S4]. Comparing theoretical simulation results with and without spin-orbit coupling [Fig. S1(d,e)] [S4], we find

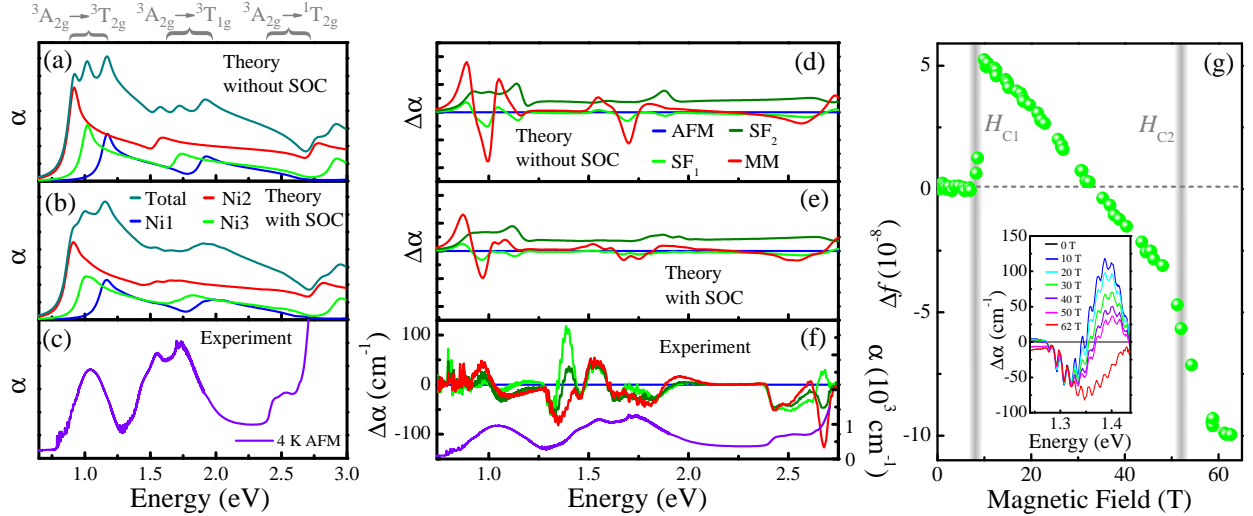


FIG. S1: Summary of the optical and magneto-optical properties of Ni_3TeO_6 in the antiferromagnetic, spin flop, and metamagnetic phases. (a, b, c) Optical absorption spectrum obtained from first principles calculations with and without spin orbit coupling as compared with the experimental absorption spectrum (α) at 4.2 K. The three different Ni centers are projected out (Ni1 in blue, Ni2 red, Ni3 green, and the total in teal). (d, e, f) Field-induced absorption difference of Ni_3TeO_6 from first principles calculations and experiment. Here, the absorption difference is defined as $\Delta\alpha = \alpha(H) - \alpha(H = 0 \text{ T})$. The absolute absorption spectrum is reproduced at the bottom of the experimental panel. (g) Oscillator strength change in the 1.3 - 1.4 eV energy region as a function of applied field. The 9 T spin-flop and 52 T metamagnetic transition are indicated. The inset shows a close-up view of the absorption difference data in the relevant energy window.

that the inclusion of spin-orbit coupling affects the magneto-optical responses significantly. As mentioned above, the features between 0.8 and 2.0 eV are blue-shifted in theory. Features around 1.6 eV are somewhat underestimated in the computed results compared to experimental observation, which is further reduced by the spin-orbit coupling. Such discrepancy between the theory and experiment in this field-induced absorption needs further analysis.

We also extracted the field-induced change in oscillator strength, Δf , over the 1.3 - 1.4 eV energy window [Fig. S1(g)] [S5]. As mentioned above, $\Delta\alpha$ in this range is substantial [inset, Fig. S1(g)]. Δf displays a sharp jump at 9 T indicating that the absorption difference is sensitive to the spin flop transition. Δf also drops across the 52 T transition to the MM phase, although not as sharply. There is certainly some smearing due to the statistics of data taking in a pulsed magnetic field, but this may also be due to the fact that (i) only half of the Ni spins are affected at the 52 T transition and (ii) only small components of magnetic moments perpendicular to the c -axis are flipped, which should not induce significant differences in terms of the local atomic configuration [S6]. In any case, the magneto-optical response of Ni_3TeO_6 is sensitive to the entire series of spin reorientations that are currently accessible in pulsed field.

Nonreciprocal effects in the raw data

Figure S2 summarizes several raw power spectra to demonstrate the clarity of the nonreciprocal effect. Focusing first on the magnetochiral orientation, we see that the 0 T spectra before the magnet pulse are exactly the same, as indicated by the pink and light blue curves. In the middle plot, the 0 T power spectrum before the pulse is maintained as a reference (black dotted curve). Here, even in the raw data it is apparent that the $+H$ and $-H$ spectra at full field are different between 1.25 and 1.4 eV. The third plot for the magnetochiral orientation is used to check for hysteresis effects. Here, we show the 0 T spectra after the magnet pulse has ramped back down compared to the 0 T data before the pulse. They match exactly, so there are no hysteresis effects.

Turning our attention to the transverse magnetochiral orientation in Fig. S2, we can see the same progression of data. Again we show the 0 T spectra before the pulse in pink and light blue. The second panel contains the full field response for the $+H$ and $-H$ pulses. At 2.0 eV, it is very obvious that the curves deviate from the 0 T results before the pulse. They also have opposite effects. The $+H$ curve has reduced transmittance whereas the $-H$ curve has increased transmittance. The last panel displays the 0 T spectra after the field pulse. Again, there are no hysteresis effects. It is important to note that the data here are the raw power spectra straight from the spectrometer. The changes are so large that they can be seen with the naked eye - without any data treatment. The light propagation direction for all of the spectra in this comparison is consistent (down k).

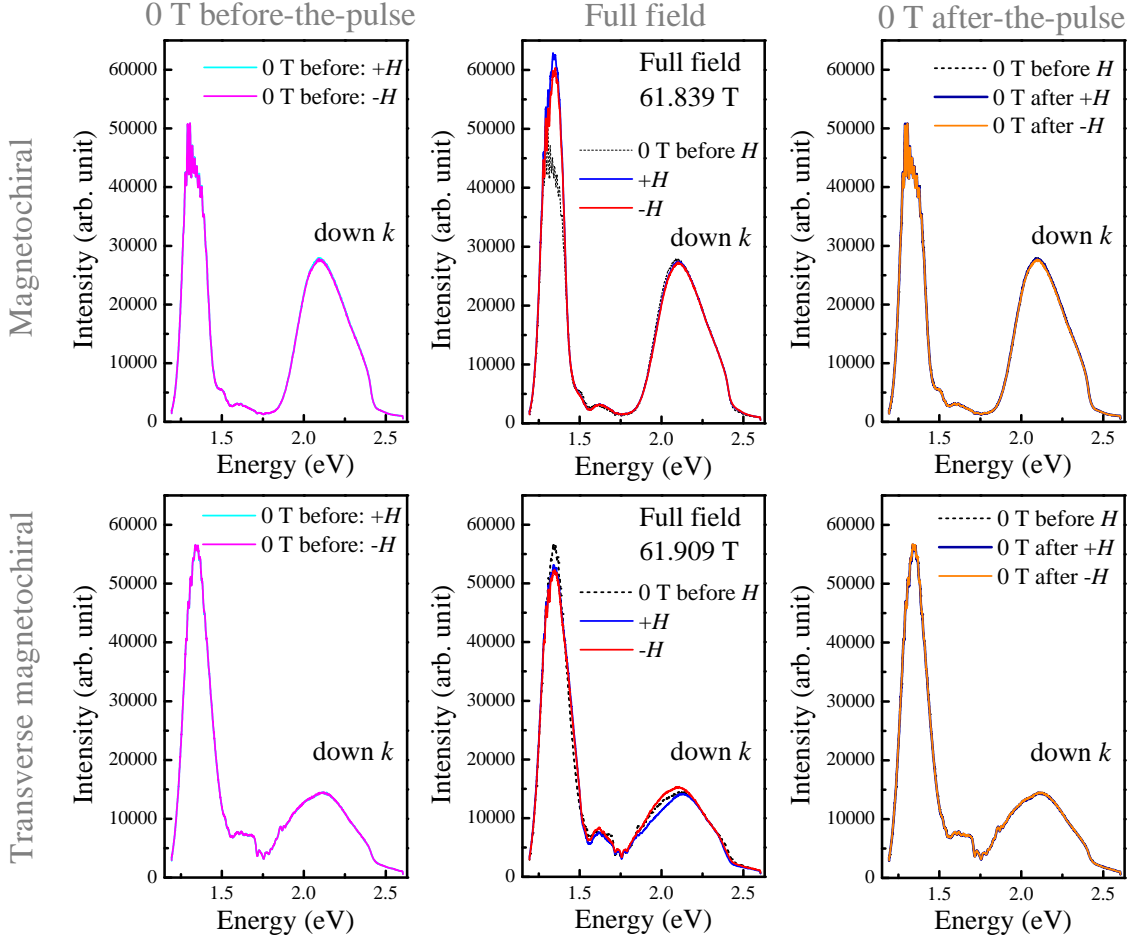


FIG. S2: Power spectra of Ni_3TeO_6 in both the magnetochiral (top) and transverse magnetochiral (bottom) orientations. The first plot in each series is the 0 T power spectra before the magnet pulse. The second plot is the full field power spectra for the respective orientations. The final plot is the 0 T power spectra after the magnet pulse compared to 0 T spectra before the magnet pulse. This eliminates hysteretic concerns.

Comparing all of the different orientations by absorption differences

In order to calculate nonreciprocal effects, we first evaluate a set of absorption difference spectra for each orientation. The four different configurations we can measure are $(+H, \text{up } k)$, $(-H, \text{up } k)$, $(+H, \text{down } k)$, and $(-H, \text{down } k)$ - all as a function of energy and magnetic field. We focus on the full field data in the meta-magnetic state here. In order to obtain an absorption difference, we take the full field power spectra and divide by the power spectra at zero field. This eliminates the reference spectrum from the final result. Here's how. Absorption is traditionally obtained as

$$\alpha_H = -\frac{1}{d} \ln\left(\frac{T_H}{T_r}\right), \text{ and} \quad (1)$$

$$\alpha_0 = -\frac{1}{d} \ln\left(\frac{T_{H_0}}{T_r}\right), \quad (2)$$

where d is the sample thickness, T_H is transmittance in the field, T_{H_0} is the transmittance at zero field, and T_r is the transmittance of the reference. To obtain $\Delta\alpha$ spectra, we calculate $(\alpha_H - \alpha_0)$. Therefore,

$$\Delta\alpha = \alpha_H - \alpha_0 = \left[-\frac{1}{d}\ln\left(\frac{T_H}{T_r}\right)\right] - \left[-\frac{1}{d}\ln\left(\frac{T_{H_0}}{T_r}\right)\right] \quad (3)$$

$$= -\frac{1}{d}\ln\left(\frac{T_H}{T_{H_0}}\right) \quad (4)$$

Thus, calculation of an absorption difference eliminates the reference.

Figure S3 summarizes the six different absorption differences that can be calculated from the four measurement configurations in Ni_3TeO_6 - for both the magnetochiral and transverse magnetochiral orientations. From these comparisons, we can see (as in the power spectra) that several of these orientations give quite different responses. Focusing first on the magnetochiral orientation [Fig. S3(a-g)], we can see many differences. Some spectra are very similar, such as in (c) and (d). Closer examination reveals that both H and k are switched. From a symmetry perspective, changing both parameters should give no nonreciprocal effect. The results are, however, very similar.

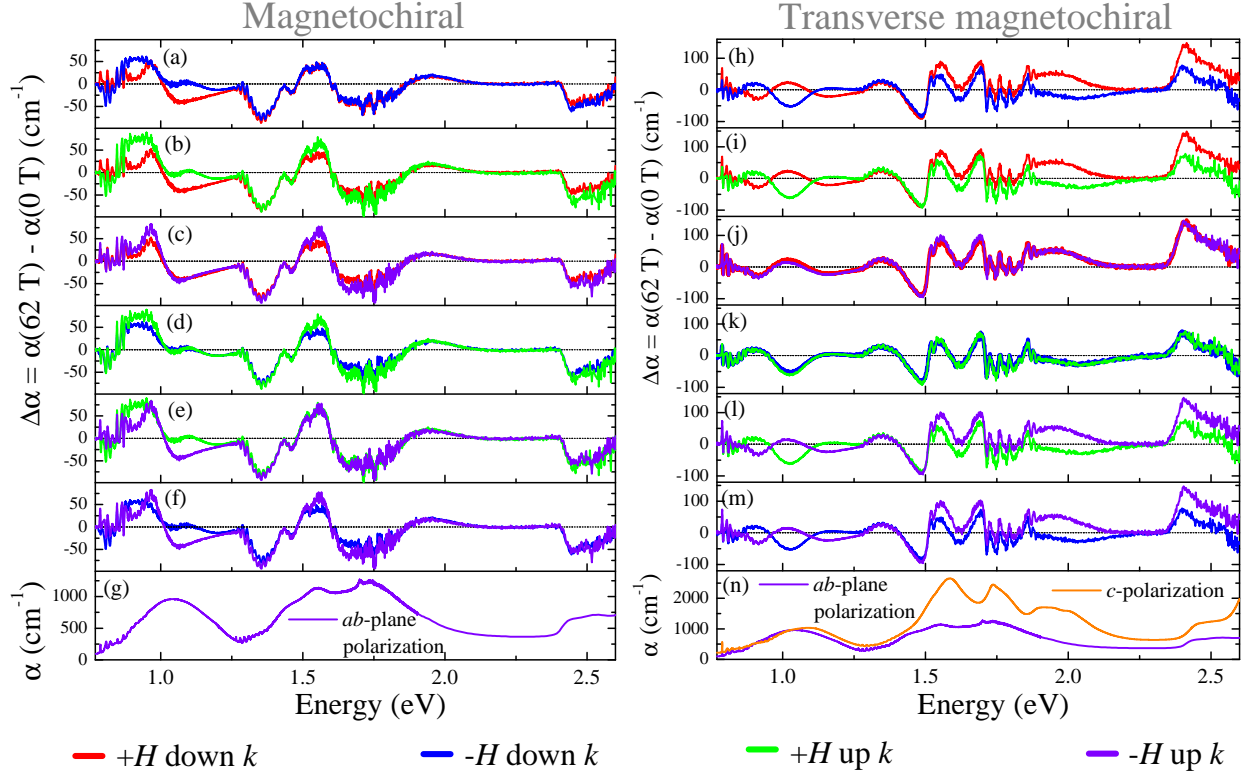


FIG. S3: Full field absorption difference ($\Delta\alpha$) spectra for each comparison are plotted, with the (+H, down k) in red, (-H, down k) in blue, (+H, up k) in green, and (-H, up k) in violet. The left most panel (a-f) is the magnetochiral orientation whereas the right most panel (h-m) is the transverse magnetochiral orientation. Here, $T = 4.0 \text{ K}$ and $H = 62 \text{ T}$. The bottom-most curves (g, n) are the linear absorption spectra at 4.2 K .

In the transverse magnetochiral orientation [Fig. S3(h-m)], there are many differences between the $\Delta\alpha$ spectra. In fact, in some regions, the curves are exactly opposite. However, in panels (j) and (k), the

curves are essentially identical. Here, we are comparing the curves when both parameters are swapped. Again, we calculate each of the six comparisons for both the magnetochiral and transverse magnetochiral orientations and subtract the $\Delta\alpha$ curves to get the nonreciprocal directional dichroism response $\Delta\alpha_{\text{NDD}}$. These results are discussed in the next section.

Comparing the nonreciprocal response of Ni_3TeO_6 in different configurations

The nonreciprocal response is defined as $\Delta\alpha_{\text{NDD}} = \alpha_{+H} - \alpha_{-H}$, where the terms $+H$ and $-H$ can be switched to $+k$ and $-k$. Since

$$\Delta\alpha_{\text{NDD}} = \Delta\alpha_{+H} - \Delta\alpha_{-H} \quad (5)$$

$$= (\alpha_{+H} - \alpha_{+H_0}) - (\alpha_{-H} - \alpha_{-H_0}) \quad (6)$$

$$= \alpha_{+H} - \alpha_{-H}, \quad (7)$$

it is clear that if the 0 T spectra are the same for each measurement ($\alpha_{+H_0} = \alpha_{-H_0}$), then finding $\Delta\alpha_{\text{NDD}}$ from absorption differences yields an accurate result. The same holds true for $\pm k$.

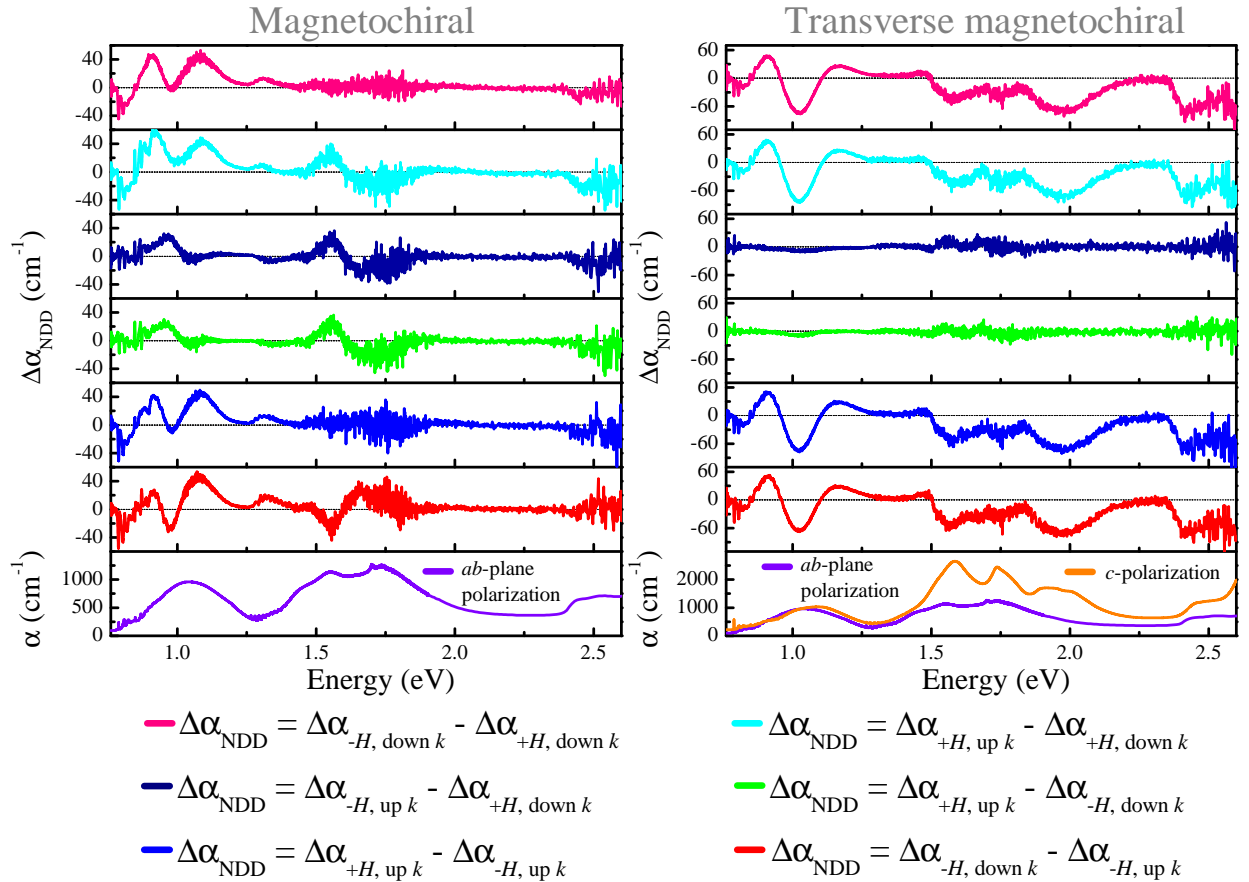


FIG. S4: $\Delta\alpha_{\text{NDD}}$ for both the magnetochiral and transverse magnetochiral orientations in Ni_3TeO_6 . Data are taken at 4.0 K and full field (62 T).

A symmetry analysis reveals that Ni_3TeO_6 can show nonreciprocity in two distinct chiral geometries

[Table S1]. This presents a unique opportunity to compare the two different versions of the magneto-chiral response in the same material. Figure S4 summarizes the $\Delta\alpha_{\text{NDD}}$ spectra. Six different comparisons can be made from the four different measurement configurations. Focusing first on the magneto-chiral orientation, we can see that most every $\Delta\alpha_{\text{NDD}}$ curve shows a response. However, two curves show a significantly smaller (and different) response than the others. These two curves are the navy and green ones, in which both parameters H and k are switched. No difference is expected based on symmetry conditions - although there is a small asymmetry that we attribute to surface charge as discussed in the main text. Turning our attention to the transverse magneto-chiral orientation, we can see the same type of response as in the magneto-chiral orientation. The major difference here is that the two curves (navy and green) that change both parameters are almost completely zero and show no nonreciprocal response. Surface charge is not an issue in this orientation because of the polarization direction.

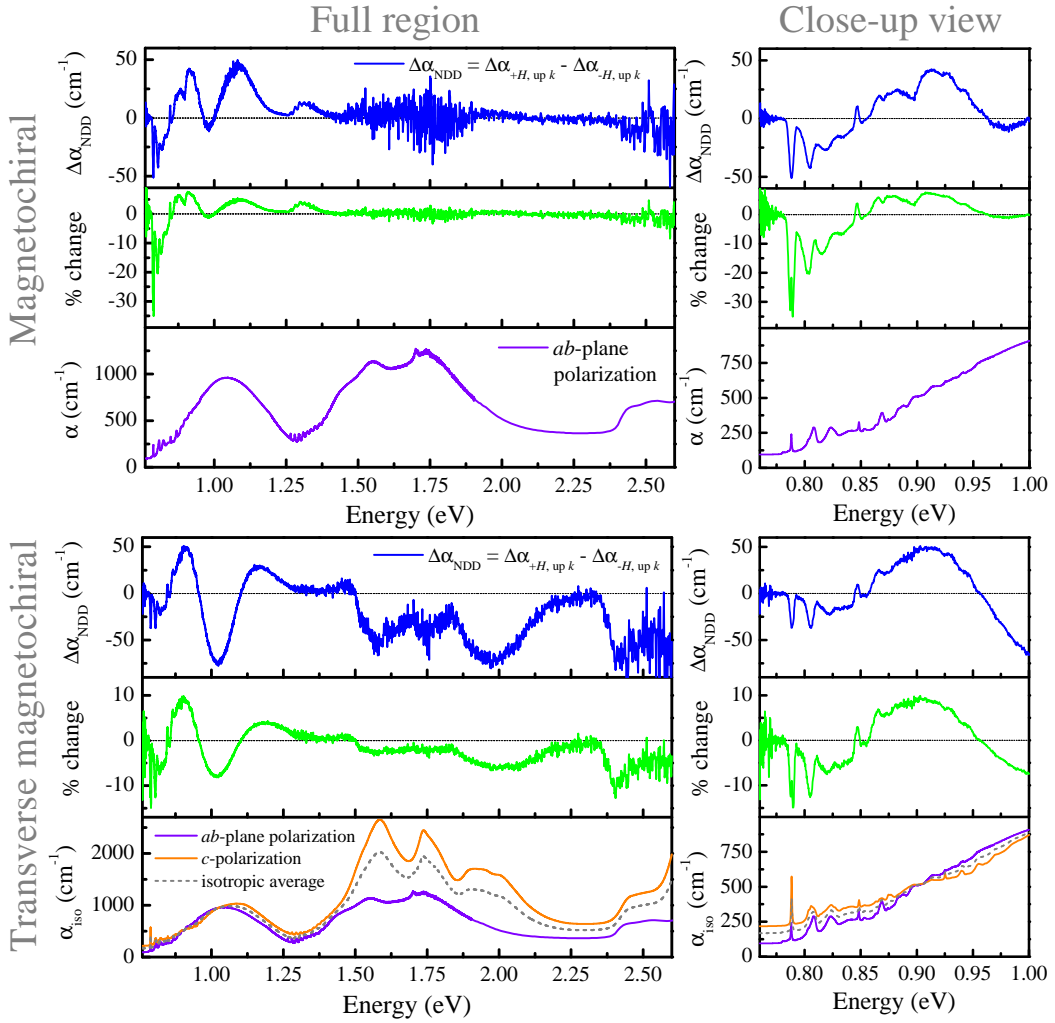


FIG. S5: Nonreciprocal effects for both the magneto-chiral (top) and transverse magneto-chiral (bottom) orientations. The middle plot in green represents the percent change of the entire observed nonreciprocal response. The right-hand panels are close-up views of the fine structure of Ni_3TeO_6 . These features are discussed in the next section.

Size of the nonreciprocal effect

To quantify the size of the nonreciprocal effect in Ni_3TeO_6 , we normalize the various spectra and plot the result as a percentage. Figure S5 demonstrates this procedure for both the magnetochiral and transverse magnetochiral orientations. For the magnetochiral orientation, we compare the nonreciprocal response to the ab -plane absorption data. Differences are as high as 35% in selected regions. Since most other materials sport magnetochiral nonreciprocal directional dichroism in the terahertz region, it is not surprising that the size of the effect can reach nearly 100% since the absorption coefficient is overall lower [S7]. For the very few cases of magnetochiral dichroism in the optical region, $\Delta\alpha_{\text{NDD}}$ is typically on the order of 10-25%. It can be up to 100% in CuB_2O_4 [S8, S9] and as small as 4.2% in CsCuCl_6 [S10].

For the transverse magnetochiral orientation, we need to normalize $\Delta\alpha_{\text{NDD}}$ by an isotropically-averaged spectrum because we are measuring both the c and $\perp c$ response. In order to calculate the percent change, we generated an “isotropic” absorption spectra (α_{iso}) by averaging the ab -plane and c -axis spectra as

$$\alpha_{iso} = \sqrt{\frac{\alpha_{ab}^2 + \alpha_c^2}{2}}. \quad (8)$$

Using this isotropically averaged absorption spectrum, we find changes as large as 15% in certain regions. Overall, the size of the nonreciprocal effect is smaller on a percentage basis in this orientation as compared to that in the magnetochiral orientation - primarily because the denominator is smaller.

Assignment and nonreciprocal response of the fine structure

As is common with antiferromagnets like MnF_2 and $\alpha\text{-Fe}_2\text{O}_3$, there is a great deal of fine structure on the leading edge of the on-site Ni d -to- d excitations at low temperature [S11-S14]. Depending on the situation, the fine structure can consist of a set of excitons, a magnon side band, or a progression of phonons. We examined a number of models in order to reveal the origin of the fine structure in Ni_3TeO_6 . One of the most useful tests was to measure how the fine structure develops with decreasing temperature. Examination of Fig. S6(a, b) immediately reveals that these excitations persist well above the 53 K ordering temperature - suggesting that they are not magnetic in origin. There is also no evidence of a magnon sideband - which is strong and broad because it is optically-allowed. A Huang-Rhys picture, in which a set of phonon sidebands are vibronically-activated and superimposed upon the leading edge of the on-site d -to- d excitation, provides a much more suitable assignment [S15, S16]. Figure S6(c) shows the infrared spectrum of Ni_3TeO_6 [S17] plotted directly underneath the optical absorption spectrum. Clearly, the former was shifted to higher energy to provide a reasonable match. This provides a very good estimate of the exciton position. In any case, examination shows that the phonons line up very well with the fine structure on the leading edge of the on-site Ni d -to- d excitation. We therefore assign the fine structure as a progression of phonon

sidebands activated by vibronic coupling. Many but not all modes are replicated. Based upon the shape of the spectra, we estimate that the Huang-Rhys factor S is approximately 3 - consistent with intermediate coupling.

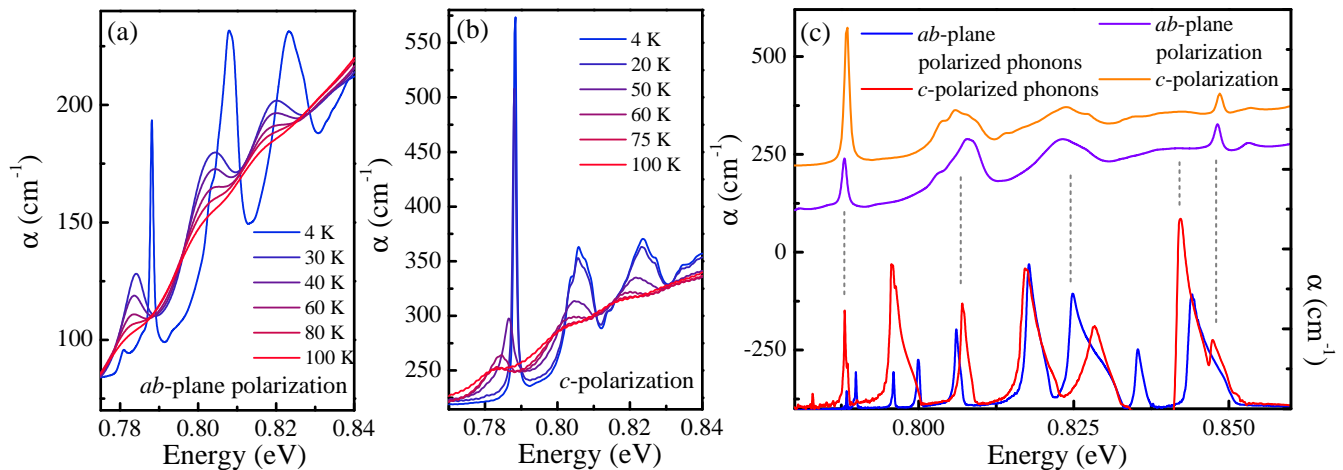


FIG. S6: (a, b) Close-up view of the fine structure on the optical absorption as a function of temperature in the ab -plane and c -direction. (c) Close-up view of the optical absorption in the vicinity of the fine structure. The phonon spectra [S17] are plotted underneath for comparison.

We now turn to the behavior of these features in magnetic field. Importantly, not every infrared-active phonon is represented in the phonon progression in Fig. S6, but every peak that is present in this progression is sensitive to applied field. As a point of comparison, direct magneto-infrared measurements show that the 310, 597, and 666 cm^{-1} modes are most sensitive to field with both frequency shifts and linewidth changes [S17]. Moreover, the features in the phonon progression are sensitive to either $\pm H$ or $\pm k$. Thus, they display a nonreciprocal response - both in the spin flop phase (above 9 T) and in the metamagnetic phase (above 52 T).

Figure S7 summarizes the nonreciprocal effect associated with the fine structure in Ni_3TeO_6 for both the magnetochiral and transverse magnetochiral configurations. The nonreciprocal response lines up well with the fine structure in the spectra. Therefore, we conclude that the phonon sidebands in Ni_3TeO_6 sport nonreciprocal effects as well. Fascinatingly, use of the phonon replicas provides a unique way of doing magneto-infrared measurements in pulsed magnetic field. Direct magneto-infrared spectroscopy can be done only to 35 T at this time in the resistive magnets at the National High Magnetic Field Laboratory. Analysis of phonon progressions may therefore be a unique way to obviate the problem in antiferromagnets. Finally, we point out that a magnetochiral mechanism is responsible for nonreciprocity of the sound velocity in Cu_2OSeO_3 [S18]. Our work is complementary but different in that we examine phonons directly (in an energy range where the fundamental excitations of the lattice reside on the leading edge of the d -to- d excitations) rather than in an averaged manner as in an ultrasound experiment. We therefore conclude

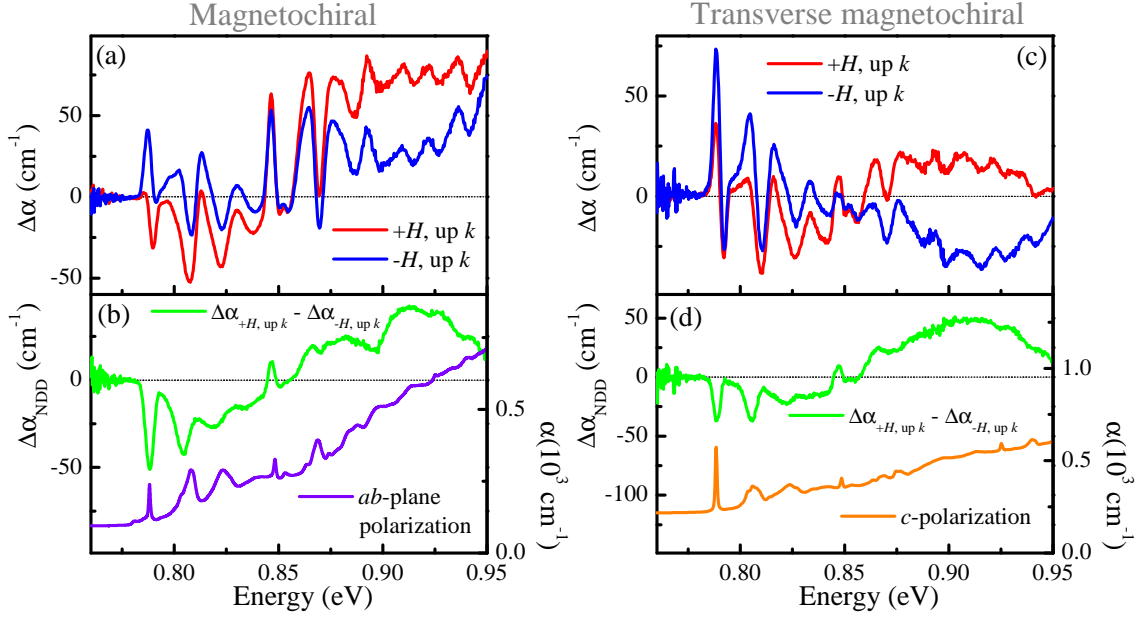


FIG. S7: (a, c) Close-up of $\Delta\alpha$ in the magnetochiral and transverse magnetochiral orientations at 4.0 K. (b, d) $\Delta\alpha_{NDD}$ in the different measurement orientations with the linear absorption spectrum plotted underneath for reference. Clearly, a number of the phonons display nonreciprocal effects.

that fundamental excitations of the lattice in the form of phonons show non-reciprocity in Ni_3TeO_6 .

* Electronic address: musfeldt@utk.edu

- [S1] Cheong, S.-W. SOS: symmetry-operational similarity. *npj Quantum Mater.* **4**, 53 (2019).
- [S2] Wang, X., Huang, F.-T., Sang, J., Oh, Y. S., & Cheong, S.-W. Interlocked chiral/polar domain walls and large optical rotation in Ni_3TeO_6 . *APL Mater.* **3**, 076106 (2015).
- [S3] Yokosuk, M. O., *et al.* Magnetolectric coupling through the spin flop transition in Ni_3TeO_6 . *Phys. Rev. Lett.* **117**, 147402 (2016).
- [S4] In the calculated results, the SF phase is separated into SF_1 and SF_2 to see how the spectrum changes from just after the spin-flop transition and directly before the metamagnetic transition.
- [S5] For the oscillator strength analysis, $\Delta f = (2c)/(N_e\pi\omega_p^2) \int_{E_1}^{E_2} n\Delta\alpha(E)dE$, where N_e is the number of electrons per Ni site, n is the refractive index, ω_p is the plasma frequency $\omega_p \equiv \sqrt{(e^2\rho)/(m\epsilon_0)}$, e and m are the charge and mass of an electron, ϵ_0 is the vacuum dielectric constant, ρ is the density of Ni sites, c is the speed of light, and E_1 and E_2 are the energy limits of integration.
- [S6] Kim, J. W., *et al.* Successive magnetic-field-induced transitions and colossal magnetolectric effect in Ni_3TeO_6 . *Phys. Rev. Lett.* **115**, 137201 (2015).
- [S7] Bordács, S., *et al.* Chirality of matter shows up via spin excitations. *Nat Phys* **8**, 734-738 (2012).
- [S8] Saito, M., Taniguchi, K., & Arima, T.-h. Gigantic optical magnetolectric effect in CuB_2O_4 . *J. Phys. Soc. Jpn.* **77**, 013705 (2008).
- [S9] Saito, M., Ishikawa, K., Taniguchi, K., & Arima, T. Magnetic control of crystal chirality and the existence of

- a large magneto-optical dichroism effect in CuB_2O_4 . *Phys. Rev. Lett.* **101**, 117402 (2008).
- [S10] Nakagawa, N., *et al.* Magneto-chiral dichroism of CsCuCl_3 . *Phys. Rev. B* **96**, 121102(R) (2017).
- [S11] Greene, R. L., Sell, D. D., Yen, W. M., Schawlow, A. W., & White, R. M. Observation of a spin-wave sideband in the optical spectrum of MnF_2 . *Phys. Rev. Lett.* **15**, 656-659 (1965).
- [S12] Sell, D. D., Greene, R. L., & White, R. M. Optical exciton-magnon absorption in MnF_2 . *Phys. Rev.* **158**, 489-510 (1967).
- [S13] Matsui, A. & Walker, W. C. Exciton and interband spectra of crystalline MnF_2 . *J. Opt. Soc. Am.* **60**, 358-365 (1970).
- [S14] Chen, P., Lee, N., McGill, S., Cheong, S., & Musfeldt, J. L. Magnetic-field-induced color change in $\alpha\text{-Fe}_2\text{O}_3$ single crystals. *Phys. Rev. B* **85**, 174413 (2012).
- [S15] Moreno, M., Barriuso, M. T., & Aramburu, J. A. The Huang-Rhys factor $S(a_{1g})$ for transition-metal impurities: a microscopic insight. *J. Phys. Condens. Matter* **4**, 9481-9488 (1992).
- [S16] Zhao, H. & Kalt, H. Energy-dependent Huang-Rhys factor of free excitons. *Phys. Rev. B* **68**, 125309 (2003).
- [S17] Yokosuk, M. O., *et al.* Tracking the continuous spin-flop transition in Ni_3TeO_6 by infrared spectroscopy. *Phys. Rev. B* **92**, 144305 (2015).
- [S18] Nomura, T., *et al.* Phonon magnetochiral effect. *Phys. Rev. Lett.* **122**, 145901 (2019).